

Large-Eddy Simulation of Non-Isothermal Flow around a Building Using Artificially Generated Inflow Turbulent Fluctuations of Wind Velocity and Air Temperature

Tsubasa OKAZE *¹ Akashi MOCHIDA *²

*¹ School of Environment and Society, Tokyo Institute of Technology

*² Graduate School of Engineering, Tohoku University

Corresponding author: Tsubasa Okaze, okaze.t.aa@m.titech.ac.jp

ABSTRACT

This study aims to apply artificially generated turbulent fluctuations of wind velocity and air temperature as inflow boundary conditions for a large-eddy simulation of a non-isothermal flow around a building. The building was an isolated high-rise structure with a length ratio of 1:1:2. The stratification condition of the flow field was weakly unstable. The artificial turbulent fluctuations generated satisfied the prescribed profiles for the turbulent fluxes of momentum and temperature. Moreover, they fulfilled the prescribed spatial and time correlations expressed using exponential functions. The mean wind velocity and mean air temperature predicted from the large-eddy simulation agreed well with the experimental results. The turbulent kinetic energy and the fluctuation of the air temperature also corresponded fairly well with the experiment except for the region immediately behind the inflow boundary.

Key Words : Inflow turbulence generation, Temperature fluctuation, Large-eddy simulation, Unstable stratification, Synthetic method, Cholesky decomposition

1. Introduction

In recent years, large-eddy simulation (LES) computations that consider the atmospheric stability in built-up environments have been reported. Generation of fluctuations of wind velocity and air temperature fluctuation used as an inflow boundary condition has become an important issue in implementing LES for non-isothermal flow fields. Kong et al.⁽¹⁾ proposed a method for generating the inflow fluctuations of wind velocity and air temperature. This method is based on the rescaling and recycling laws for the flow field proposed by Lund et al.⁽²⁾ and is extended to the temperature field. Hattori et al.⁽³⁾ conducted direct numerical simulations for very weak unstable and stable boundary layers using the method proposed by Kong et al.⁽¹⁾ to generate inflow turbulent fluctuations of wind velocity and air temperature. Jiang et al.⁽⁴⁾ performed LESs for boundary layers, both weakly stable and weakly unstable stratifications, using Kataoka's recycling method⁽⁵⁾ to generate inflow turbulence and air temperature fluctuations. Tamura et al.⁽⁶⁾ conducted an LES for a non-isothermal flow field in the Tokyo metropolitan area with inflow turbulence and air temperature fluctuations. A driver

region was established consisting of two domains in the preliminary calculation for generating inflow turbulence and air temperature fluctuations. Matsuda et al.⁽⁷⁾ investigated the greenery effect in the Tokyo Bay area using LES. They set a long approaching section over the Tokyo Bay to generate the wind velocity and air temperature fluctuations. However, the methods for generating the velocity and temperature fluctuations based on a preliminary or additional LES need additional computational costs in the preliminary or additional calculations. Furthermore, in these methods, the distributions of mean wind velocity and air temperature and its fluctuations are obtained after the preliminary computation. This means it is not easy to impose the prescribed profiles of wind velocity, air temperature and the turbulent fluxes of the momentum and air temperature. Thus, the process of the trial and error is usually needed. Recently, the present authors proposed a method for generating turbulent fluctuations of wind velocity and various scalar quantities, such as air temperature and contaminant concentration, based on Cholesky decomposition of the time-averaged turbulent flux tensors of momentum and scalar quantities⁽⁸⁾. The artificial turbulent fluctuations generated using

this method satisfy both the prescribed profiles for the turbulent fluxes of momentum and the considered scalar quantities. The authors then confirmed the flow field and dispersion of a passive scalar in a boundary layer were well reproduced with artificially generated inflow boundary conditions, including wind velocity and passive scalar fluctuations. Nevertheless, the performances of artificially generated fluctuations of wind velocity and air temperature in a non-isothermal flow field have not been investigated.

The objective of this study was to therefore apply artificially generated turbulent fluctuations of wind velocity and air temperature as inflow boundary conditions for a large-eddy simulation of a non-isothermal flow field around an isolated high-rise building. The LES results were compared with those of a wind tunnel experiment.

2. Overview of inflow turbulence generation and scalar fluctuation

We developed an artificial generation method of the fluctuations of wind velocity and scalar based on Cholesky decomposition of the Reynolds stress tensor and turbulent scalar flux⁽⁸⁾. In this study, the proposed method was employed to generate the wind velocity and air temperature fluctuations for LES inflow boundary conditions.

The proposed method is summarized as follows. The wind velocities and scalars are expressed as f_i , the time-averaged values of f_i are denoted as $\langle f_i \rangle$, and the deviations from the time-averaged value are expressed as f_i' :

$$f_i = \langle f_i \rangle + f_i', \quad (1)$$

where the subscripts, $i = 1, 2, 3$, represent the wind velocity components in the streamwise, lateral, and vertical directions (u , v , w), respectively, and $i = 4$ represents the scalar value, ϕ . A regular matrix of the turbulent fluxes of the momentum and scalar, R_{ij} , is defined as

$$R_{ij} = \begin{pmatrix} \langle u'u' \rangle & \langle u'v' \rangle & \langle u'w' \rangle & \langle u'\phi' \rangle \\ \langle v'u' \rangle & \langle v'v' \rangle & \langle v'w' \rangle & \langle v'\phi' \rangle \\ \langle w'u' \rangle & \langle w'v' \rangle & \langle w'w' \rangle & \langle w'\phi' \rangle \\ \langle \phi'u' \rangle & \langle \phi'v' \rangle & \langle \phi'w' \rangle & \langle \phi'\phi' \rangle \end{pmatrix}. \quad (2)$$

The Cholesky decomposition of R_{ij} produces a lower triangular matrix, a_{ij} :

$$a_{ij} = \begin{pmatrix} \sqrt{R_{11}} & 0 & 0 & 0 \\ R_{21}/a_{11} & \sqrt{R_{22}-a_{21}^2} & 0 & 0 \\ R_{31}/a_{11} & R_{32}-a_{21}a_{31}/a_{22} & \sqrt{R_{33}-a_{31}^2-a_{32}^2} & 0 \\ R_{41}/a_{11} & R_{42}-a_{21}a_{41}/a_{22} & R_{43}-a_{31}a_{41}-a_{32}a_{42}/a_{33} & \sqrt{R_{44}-a_{41}^2-a_{42}^2-a_{43}^2} \end{pmatrix}. \quad (3)$$

With a_{ij} and a variable Ψ_j that satisfies $\langle \Psi_j \rangle = 0$ and $\langle \Psi_i \cdot \Psi_j \rangle = \delta_{ij}$, the fluctuations, f_i , can be rewritten as

$$f_i = \langle f_i \rangle + f_i' = \langle f_i \rangle + a_{ij} \Psi_j. \quad (4)$$

The transformation originally proposed by Le and Moin⁽⁹⁾ uses

Reynolds stress tensors as a 3×3 matrix. Here, it is extended to account for the turbulent fluxes of a scalar within a 4×4 matrix. To impose time and space correlations for each component of the fluctuation, a two-dimensional digital-filter method proposed by Xie and Castro⁽¹⁰⁾ is employed. The prescribed time and space correlations are assumed using exponential functions with an integral time scale, T , and a length scale, L :

$$\frac{\langle \Psi_j(t) \Psi_j(t+\tau) \rangle}{\langle \Psi_j(t) \Psi_j(t) \rangle} = \exp\left(-\frac{\pi\tau}{2T}\right), \quad (5)$$

and

$$\frac{\langle \Psi_j(r) \Psi_j(r+\lambda) \rangle}{\langle \Psi_j(r) \Psi_j(r) \rangle} = \exp\left(-\frac{\pi\lambda}{2L}\right). \quad (6)$$

The update equation for the artificially generated fluctuations on a grid point (m, n) is expressed as

$$\Psi_j(t+\Delta t, m, n) = \Psi_j(t, m, n) \exp\left(-\frac{\pi\Delta t}{2T}\right) + \psi_j(t+\Delta t, m, n) \left\{ 1 - \exp\left(-\frac{\pi\Delta t}{T}\right) \right\}^{1/2}, \quad (7)$$

where

$$\psi_j(t, m, n) = \sum_{m'=-N_y}^{N_y} \sum_{n'=-N_z}^{N_z} b_m b_n r_{m+m', n+n'}. \quad (8)$$

Here, r is a random number satisfying $\langle r_j \rangle = 0$ and $\langle r_i r_j \rangle = \delta_{ij}$, N_y and N_z relate to the length scale of the filter in each direction, and b_k is a digital-filter coefficient for the integral length scale in the generated plane in each direction, as described below:

$$b_k = \tilde{b}_k / \left(\sum_{j=-N}^N \tilde{b}_j^2 \right)^{1/2}, \quad (9)$$

where

$$\tilde{b}_k = \exp\left(-\frac{\Delta x |k|}{L}\right). \quad (10)$$

By substituting ψ_j (as obtained using the new dataset of random numbers from Eqs. (8) to (10)) into Eq. (7) for each time step, Ψ_j for the next time step is obtained. Then, the fluctuations, f_i , are given by substituting Ψ_j into Eq. (4).

3. LES of non-isothermal flow around a building

3.1. Calculation conditions

For LES validation data, we selected a wind tunnel experiment for a non-isothermal flow field around an isolated high-rise building model with dimensions $D \times D \times 2D$ ($H = 2D$) in the streamwise (x), lateral (y), and vertical (z) direction, respectively. It was conducted in a thermally stratified wind tunnel at Tokyo Polytechnic University⁽¹¹⁾. The stratification of the approaching flow was weakly unstable. The total measurement points were 260. Of these points, 152 were in the vertical center section, $y = 0.0 H$. Another 108 points were located on the horizontal plane at $z = 1/4 H$.

The bulk Richardson number, R_i , is -0.10 and is defined as $R_i = (g / \Theta_0) \cdot (\Delta\Theta / \delta) / (U_\delta / \delta)^2$. Here, δ is the boundary layer height, and U_δ and Θ_δ denote the mean streamwise wind velocity and air temperature at the boundary layer height, respectively. Θ_f represents the mean temperature of the wind tunnel floor, $\Delta\Theta$ is the temperature difference between Θ_δ and Θ_f . $\Theta_\delta - \Theta_f$, Θ_0 denotes the mean air temperature in the boundary layer, and g is the gravity acceleration.

Fig. 1 illustrates the computational domain. The computational domain was set to $12.5H(x) \times 6.0H(y) \times 5.0H(z)$, where H is the building height. The cross section of the computational domain corresponds to that of the wind tunnel. An orthogonal grid system was applied. The calculation conditions are summarized in Table 1. LES was performed with OpenFOAM ver.2.4.0⁽¹²⁾. The standard Smagorinsky model was used for the sub-grid scale turbulence model. The Smagorinsky constant was set to 0.12. The building width and height were uniformly discretized into 20 and 40 with computational grids, respectively. The grid size was expanded at a distance from the building with an expansion ratio of 1.08. A second-order linear-interpolation scheme was used for the diffusion terms. In convection terms,

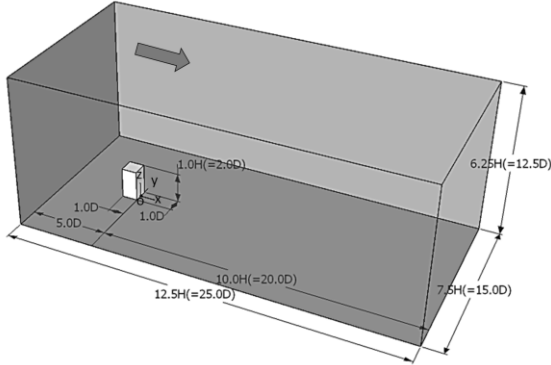


Figure 1: Computational domain

Table 1: Calculated conditions

Computational domain	$12.5 H(x) \times 7.25 H(y) \times 6.5 H(z)$
Grid arrangement	$147(x) \times 114(y) \times 90(z)$
SGS model	Standard Smagorinsky model ($C_s = 0.12$)
Time advancement	First-order backward
Inlet boundary	Artificially generated fluctuations based on the method proposed in Section 2
Outlet boundary	Advective outflow condition
Upper and side boundaries	Flow field: Slip wall Temperature field: Adiabatic condition
Ground and building boundaries	Flow field: a two-layer model based on the linear-power law expression proposed by Werner and Wengle ⁽¹³⁾ was used to estimate wall shear stress. Temperature field: The wall temperatures were fixed with the experimental result. A two-layer model based on the linear-power law expression proposed by Tuchiya et al. ⁽¹⁴⁾ was used to estimate heat flux on the walls.
Reynolds number	$1.5 \times 10^4 (\langle u_H \rangle \times H / \nu)$

the first-order upwind scheme was automatically mixed to 40% when the convection boundedness criterion was violated to avoid the appearance of unphysical oscillations in the result. This scheme was implemented as “filteredLinear2V” in OpenFOAM⁽¹²⁾. Fluctuations of wind velocity and air temperature for the LES inflow boundary condition were artificially generated at intervals of $1/16 H$ on the inflow boundary ($7.5 H (y) \times 6.25 H (z)$) based on the method described in Section 2. The characteristic turbulent length, L , in each component of wind velocity was assumed to be a constant value, 0.15δ , where δ is the boundary layer height. The characteristic time scale, T , was calculated from L and the mean streamwise wind velocity at the boundary layer height U_δ based on Taylor’s hypothesis of frozen turbulence, $T = L / U_\delta$. The turbulent length and time scales of the air temperature were assumed to be same values of these of wind velocity in this study.

A run-up calculation was performed over $t^* = 200$ with dimensionless time, t^* , which is defined as $t^* = t \times \langle u_H \rangle / H$. Here, t is the time calculation, and $\langle u_H \rangle$ denotes the mean wind velocity at the building height of the inflow boundary. From that point, the turbulent statistics were collected and averaged over $t^* = 400$ as the main simulation.

3.2. Results and discussion

The wind velocity and turbulent statistics were normalized with the mean wind velocity at the building height of the inflow boundary $\langle u_H \rangle$ and building height H . The air temperature was normalized with the temperature difference between the mean

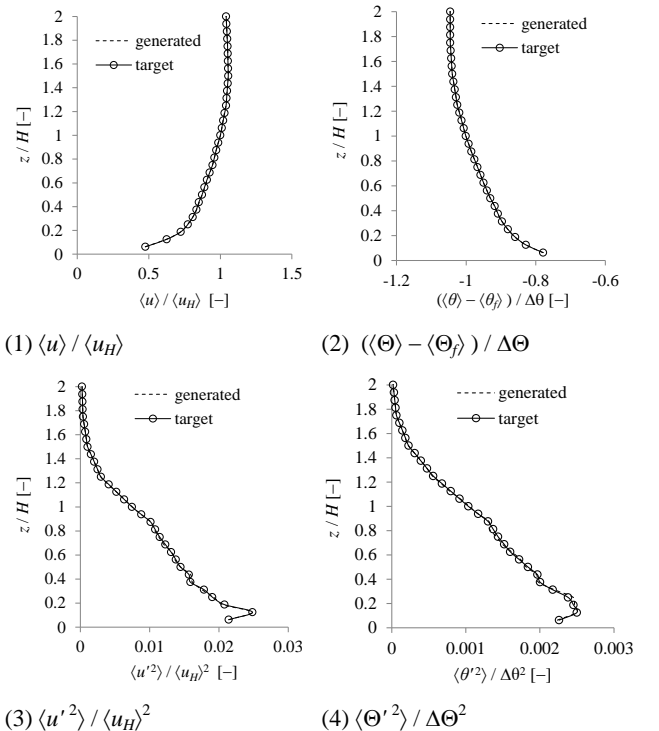
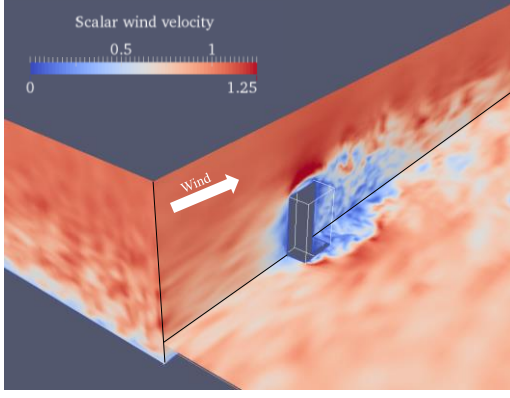
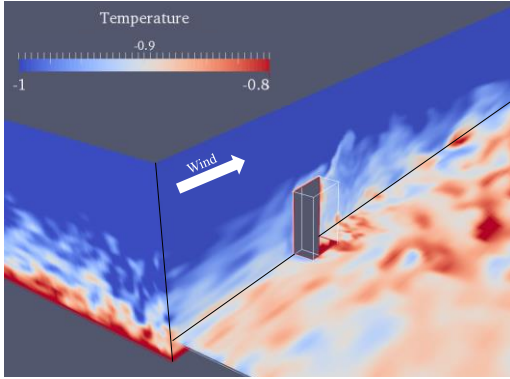


Figure 2: Comparison of targeted values and artificially generated values for inflow boundary condition



(1) Scalar wind velocity



(2) Air temperature

Figure 3: Distributions of instantaneous scalar wind velocity and air temperature at $x = -2.5 H$ (inflow boundary), $y = 0 H$ (center section) and $z = 0.25 H$

temperature of the floor and that of the building height at the inflow boundary ($\langle \Theta_f \rangle - \langle \Theta_H \rangle$).

Fig. 2 shows a comparison between the targeted values and the artificially generated values for the inflow boundary condition based on the method in Section 2. The generated mean wind velocity and air temperature completely agree with the targeted values. The variance of the fluctuation of streamwise component of wind velocity and the fluctuation of air temperature are also in good agreement with the targeted values. Thus, we confirmed that the generated turbulent fluctuations, as obtained by this proposed method, satisfy the prescribed time-averaged values.

Fig. 4 illustrates the distributions of scalar wind velocity and air temperature at $x = -2.5 H$ (inflow boundary), $y = 0 H$ (center section) and $z = 0.25 H$. The spatial heterogeneities of wind velocity and air temperature were observed at the planes $y = 0 H$ and $z = 0.25 H$. The fluctuations generated on the inflow boundary were advected to the downstream region. On the leeward areas of strong wind regions on the building side, the flow near the floor was elevated. Then, the high temperature air was transported to the upper region and the high temperature areas were scattered on the leeward of the strong wind region. The streamwise component of the mean wind velocity and mean air temperature obtained from LES were compared with those

from the wind tunnel experiment shown in Fig. 3. The mean wind velocity and air temperature predicted from LES agreed very well with those of the experiment. The degree of agreement between the experimental and LES results was evaluated by the hit rate⁽¹⁵⁾ and a factor of two of observations (FAC2)⁽¹⁶⁾. Evaluated values of these two validation metrics are compared in Table 2. The hit rate, q , is used as a metric by the German VDI Guideline⁽¹⁵⁾ for the comparison of velocities, and it is calculated from

$$q = \frac{1}{N} \sum_{i=1}^N n_i$$

$$\text{with } n_i = \begin{cases} 1 & \text{for } \left| \frac{P_i - O_i}{O_i} \right| < D \\ 1 & \text{for } \left| \frac{P_i - O_i}{P_i} \right| < W \\ 0 & \text{else} \end{cases} \quad (11)$$

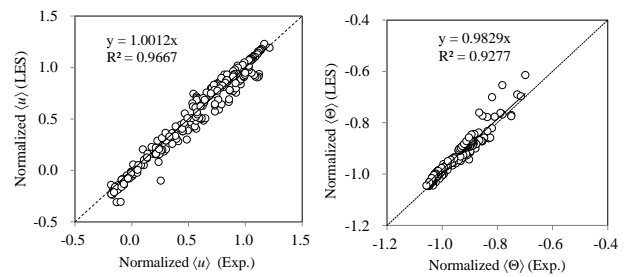
while FAC2 is evaluated using

$$\text{FAC2} = \frac{1}{N} \sum_{i=1}^N n_i$$

$$\text{with } n_i = \begin{cases} 1 & \text{for } 0.5 \leq \frac{P_i}{O_i} \leq 2 \\ 1 & \text{for } |O_i| \leq W \text{ and } |P_i| \leq W \\ 0 & \text{else} \end{cases} \quad (12)$$

Here, N is the total number of measurement points, O is the observation result, and P is the predicted result. In this study, D and W were set to 0.25 and 0.05, respectively.

Table 2 shows the metrics evaluated for the streamwise component of the mean wind velocity and turbulent kinetic energy (TKE). According to the VDI guideline⁽¹⁵⁾, the limit $q \geq 0.66$ could be used as the quality acceptance criterion. The metrics are high for the streamwise component of the mean wind velocity. However, the TKE has relatively low metrics.



(1) Streamwise component of mean wind velocity (2) Mean temperature

Figure 4: Comparison of experimental results with LES results

Table 2: Validation metrics with q and FAC2

	q	FAC2
Streamwise component of mean wind velocity	0.87	0.98
TKE	0.44	0.77

Furthermore, Fig. 5 shows the distributions of the streamwise component of the mean wind velocity, mean air temperature, TKE, and the variance of temperature fluctuation in vertical lines at $x = -1.0 H, 0.0 H, 1.0 H,$ and $2.0 H,$ and $y = 0.$ The mean wind velocity and air temperature predicted from LES agree very well with those of the experiment. TKE corresponds relatively well with the experiment, except for just behind the inflow boundary. TKE decreased by 40% of the imposed value as the inflow boundary condition immediately behind the inflow boundary.

The cause of the above decrease of TKE likely relates to the

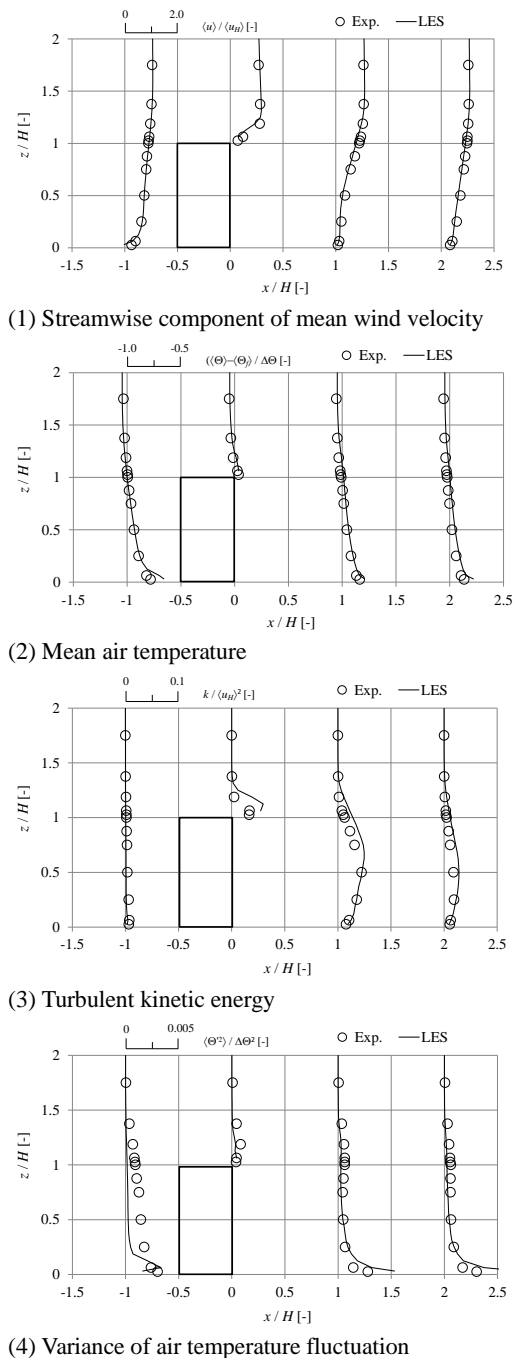


Figure 5: Distributions of statistics in vertical lines at $x = -1.0 H, 0.0 H, 1.0 H$ and $2.0 H$

fact that the artificially generated velocity fluctuations do not satisfy the continuity and momentum equations, as shown by Xie and Castro⁽¹⁰⁾. The variance of air temperature fluctuation agrees well with the experiment, except for behind the inflow boundary. The distribution of the variance of air temperature fluctuation shows a similar trend as the distribution of TKE behind the inflow boundary. The variance rapidly decreased, similar to the decrease of TKE.

4. Conclusions

In this study, a time series of wind velocity and air temperature fluctuations was generated based on the Cholesky decomposition of the Reynolds stress tensor and turbulent heat flux. The artificially generated fluctuations were used as the inflow boundary condition of LES of flow around a building model under a weakly unstable condition.

The mean wind velocity and air temperature predicted by LES using the generated inflow turbulence were generally in good agreement with the experimental results.

Although TKE decreased by 40% of the imposed value as the inflow boundary condition immediately behind the inflow boundary, TKE and the variance of air temperature fluctuation agreed reasonably well with the experiment, except for the region immediately behind the inflow boundary.

Acknowledgement

The authors are grateful for the support provided by the Grant-in-Aid for Scientific Research (C) (Grant No. 26420578).

References

- (1) Kong H., Choi H., Lee J.S., Direct numerical simulation of turbulent thermal boundary layers. *Phys. Fluids*, 12 (2000).
- (2) Lund T.S., Wu X., Squires K.D., Generation of Turbulent Inflow Data for Spatially-Developing Boundary Layer Simulations. *J. Comput. Phys.*, 258 (1998), pp. 233-258.
- (3) Hattori H., Houra T., Nagano Y., Direct numerical simulation of stable and unstable turbulent thermal boundary layers. *Int. J. Heat Fluid Flow*, 28 (2007), pp.1262-1271.
- (4) Jiang G., Yoshie R., Shirasawa T., Jin X., Inflow turbulence generation for large eddy simulation in non-isothermal boundary layers. *J. Wind Eng. Ind. Aerodyn.*, 104 (2012), pp.369-378.
- (5) Kataoka H., Mizuno M., Numerical flow computation around aeroelastic 3D square cylinder using inflow turbulence. *Wind Struct.*, 5 (2002), pp.379-392.
- (6) Tamura T., Nozu T., Okuda Y., Ohashi M., Umakawa H. Hybrid method of meteorological and LES models for heat environment. *Proc. 8th Int. Conf. Urban Clim.*, (2012), Dublin, Ireland.

- (7) Matsuda K, Onishi R, Takahashi K. High-resolution large-eddy simulations for analyzing greenery effect in Tokyo Bay Zone. 8th proc. Japanese-German Meet. Urban Climatol., (2017), pp. 69-72, Osaka Japan.
- (8) Okaze T., Mochida A. Generation of artificial inflow turbulence including scalar fluctuation for LES based on Cholesky decomposition. Proc. 9th Int. Conf. urban Clim., (2015), Toulouse, France.
- (9) Le H, Moin P. Direct numerical simulation of turbulent flow over a back-facing step. Rep TF-58 (1994), Thermosciences Div., Stanford Univ.
- (10) Xie Z.T., Castro I.P. Efficient Generation of Inflow Conditions for Large Eddy Simulation of Street-Scale Flows. Flow, Turbul. Combust., 81 (2008), pp. 449-470.
- (11) Yoshie R., Jiang G., Shirasawa T., Chung J., CFD simulations of gas dispersion around high-rise building in non-isothermal boundary layer. J. Wind Eng. Ind. Aerodyn., 99 (2011), pp.279-288.
- (12) OpenFOAM User Guide (2014), <http://openfoam.org/>.
- (13) Werner H., Wengle H. Large-eddy simulation of turbulent flow over and around a cube in plate channel. Proc. 8th Symp. Turbul. Shear Flows, (1991), pp.155-158.
- (14) Tsuchiya N., Iizuka S., Ooka R., Murakami S., Kato S. Analysis of turbulence structure of a non-isothermal room airflow through budgets of Reynold stresses and turbulent heat fluxes based on LES database. J. Archit. Plann. Environ. Eng., AIJ, 550 (2001), pp.47-54.
- (15) VDI. Environmental meteorology - Prognostic microscale wind field models evaluation for flow around buildings and obstacles, VDI Guideline 3783, Part 9, (2005), pp.53.
- (16) Schatzmann M., Olesen H., Franke J.. COST 732 model evaluation case studies: approach and results, (2010), COST Action.

(Received Apr. 29, 2017, Accepted Jul. 7, 2017)